Improvement of Electrochemical Properties of Ni/CuO Nanocomposites for Efficient Supercapacitor Applications

M. Seethalakshmi[1], M. Shanthi[2,*], S. Dhanapandian[1] and K. Ashokkumar[3]

[1]Department of Physics, Annamalai University, Annamalainagar-608002, India
[2]Department of Physics, Government Arts College for Women, Sivagangai-630562, India
[3]Department of Physics, V.R.S. College of Engineering & Technology, Arasur, Villupuram-607107, India

*Corresponding author: E-mail: shanthi9962562962@gmail.com

In this work, Ni@CuO nanocomposites were prepared *via* the low-temperature hydrothermal method for supercapacitor applications. The formation of Ni@CuO nanocomposite have been confirmed by XRD, FTIR, SEM, BET and XPS techniques. X-ray diffraction peaks were revealed the cubic structure of the Ni@CuO nanoparticles with calculated crystallite size value of 11.37 nm, whereas the SEM images revealed the spherical-like surface morphology of synthesized products. Fourier transform infrared spectrum (FTIR) studies exhibit the presence of chemical bonds, vibrating at characteristic frequencies and vibrational bands at 1000 cm^{-1} ascribed to the metal bonds. The chemical bonding/oxidation state effects were considered by XPS analysis. CV measurement of Ni@CuO electrode shows a high C_{sp} value obtained of 374 F/g at 10 mV/s. Over modified synthesized powder material showed significant enhancement in stability and showed the maximum retention value of 88.54% prepared electrode. Furthermore, the EIS measurement exposed the outstanding rate capability and reversible nature. This work gives a new pathway and highly desirable to development of high-performance pseudocapacitance nature and is suitable material for electrode fabrication of the Ni@CuO nanocomposite.

Keywords: Ni@CuO nanocomposite, Electrochemical studies, Hydrothermal method, Supercapacitor.

INTRODUCTION

In modern era, the growth of global energy demands and their associated environmental impact have been promoted and there is a well-established need for new energy technologies by the researchers [1]. To meet the continuous needs for energy storage, supercapacitors have become one of the key electrochemical energy storage solutions. The most promising near-term future markets for next-generation energy devices are due to their main advantages, *i.e.*, long cycle life, high power density, environment friendly, fast charging and discharging, excellent cycle stability and a relative stability of their temperature characteristics with respect to the batteries, such as consumption of unsustainable energy and pollution of the environment [2,3]. The two mechanisms are used for super-capacitive behaviour, which is able to store more energy. Generally, the first mechanisms are the pseudocapacitors based material depending on their charge storage mechanisms with typical pseudocapacitive materials and the electrochemical

double layer capacitor (EDLC) with carbon materials provided by electrostatic charge build-up at the electrode/electrolyte interface [4]. The carbon electrode materials are major in EDLC such as activated carbon, carbon nanotubes (CNT) and graphene.

In recent years, researchers have focused on electrochemical behaviour in transition metal oxides (MOs), including RuO$_2$, NiO, Fe$_2$O$_3$, CO$_3$O$_4$, Cr$_2$O$_3$, MnO$_2$, *etc*. Among them, the transition metal oxides are tested, in which copper oxide exhibits brilliant electrochemical performance and leads to much higher specific capacitance in nature [5,6]. Pseudocapacitors are indispensable energy storage devices with superior properties such as fast recharge rate, excellent specific power and prolong life-cycle, are used in camera (flash equipment), cellular phones, hybrid vehicles applications, *etc.* [7]. The supercapacitors performance were improved by means of innovative electrode materials possessing pathways/channels for ion intercalation and good understanding of ion storage mechanism [8]. In recent years MnO$_2$, RuO$_2$, SnO$_2$, Fe$_2$O$_3$, CuO and NiO$_2$ have been most extensively used materials for energy storage applications

owing to their low cost, natural abundance and eco-friendliness [9,10].

Commonly, nickel composite is mainly considered as the approach to improve the conductivity of copper oxide electrode material [11]. The electrochemical performance of the super-capacitors has greatly improved by surface area, pore size/distribution, particle size, morphology and crystallinity of the prepared product [12]. Although several CuO nanoparticles have been successfully prepared, the growth mechanism and the correlation between the structure and electrochemical activity are still in its infancy [13]. CuO nanostructures can be produced with various methods, including sol-gel synthesis [14], co-precipitation [15] and the hydrothermal method [16]. Herein, the hydrothermal method has many advantages over other con-ventional methods owing to its high-pressure, control of cryst-allite sizes and morphologies and non-polluting nature [17]. In this work, Ni@CuO nanocomposites were prepared through the high-pressure hydrothermal method. The crystallite size, morphologies and functional group are carried out XRD, SEM and FTIR. Further, the electrochemical behaviour of prepared nanocomposites was analyzed by cyclic voltammetry (CV), galvanostatic charge discharge (GCD) and electrochemical impedance spectroscopy (EIS).

EXPERIMENTAL

Copper nitrate hexahydrate, polyethylene glycol (PEG), nickel chloride hexahydrate, sodium hydroxide were of analy-tical reagent grade and procured from various reputed commer-cial chemical suppliers. Double distilled water was used through-out the experiments.

Preparation of bare and Ni@CuO nanocomposites: The bare and Ni@CuO nanostructures (Ni = 30%, 40% and 50%) were synthesized by hydrothermal method. Copper nitrate (1 M) was dissolved in 40 mL of double distilled water and magnetically stirred. After that 0.05 M of PEG template added in 40 mL of double distilled water in two separate beakers and the above solution was stirred to homogenous by 20 min. After that, 30% of $NiCl_2$ was mixed in 40 mL double distilled water.

Then, a precipitate agent of 0.4 M NaOH was mixed with double distilled water that the solution added dropwise into above solution. The composite solution was continuously stirred to get an obvious, crystal clear solution. After that the mixer solution was finally shifted into a 150 mL of autoclave. Then the autoclave was sealed and kept in oven for 170 ºC for 6 h. Finally, the obtained digested material was filtered and washed with ethanol to remove moisture. Furthermore, the precipitate was dried and used in an oven for 6 h at 100 ºC. A similar procedure was followed with 40% (Ni) and 50% (Ni).

Characterization: The crystallographic property of syn-thesized composite product was conducted by X-ray powder diffraction meter (XRD-6000, Shimadzu) and recorded from $2\theta = 20º$ to 80º with Cu$K\alpha$ radiation source ($\lambda = 1.5406$ Å). The surface morphology, nanostructure information, particle size and presented elements were identified by SEM with EDAX instrument (JSM-6360LA). The exits chemical bonding was studied from 4000-400 cm^{-1} by FTIR spectrometer (RX1 Perkin Elmer Spectrum 2) using KBr pellets. The active surface area and porosity was analyzed by BET model (Micromeritics-ASAP 2020). The surface electron state and chemical composition have been tested by XPS (Thermo-Fisher). The electrochemical behaviour was measured at various independent scan rate in an electrochemical analyzer (CHI 660).

RESULTS AND DISCUSSION

Structural studies: The XRD spectra of bare CuO and Ni@CuO nanocomposites are shown in Fig. 1. The cubic structure is obtained from the diffraction peaks. The diffraction peaks obtained at $2\theta = 35º, 38º, 42º, 58º, 61º, 65º, 68º, 72º$ and 74º are due to bare CuO while $2\theta = 15.9º$ and 19º correspond to Ni. They could be matched with JCPDS card no. 77-1898 and 02-1216, which are CuO and Ni, respectively [18,19]. Intensity of the peaks increased while the width is decreased within increase Ni (30%, 40% and 50%) concentration due to enhanced crystallinity [20]. The crystallite sizes of Ni@CuO are decreased as a result of substitutional defects due to incorpor-ation by Ni^{2+} ions in the host lattice that the CuO lattice sites
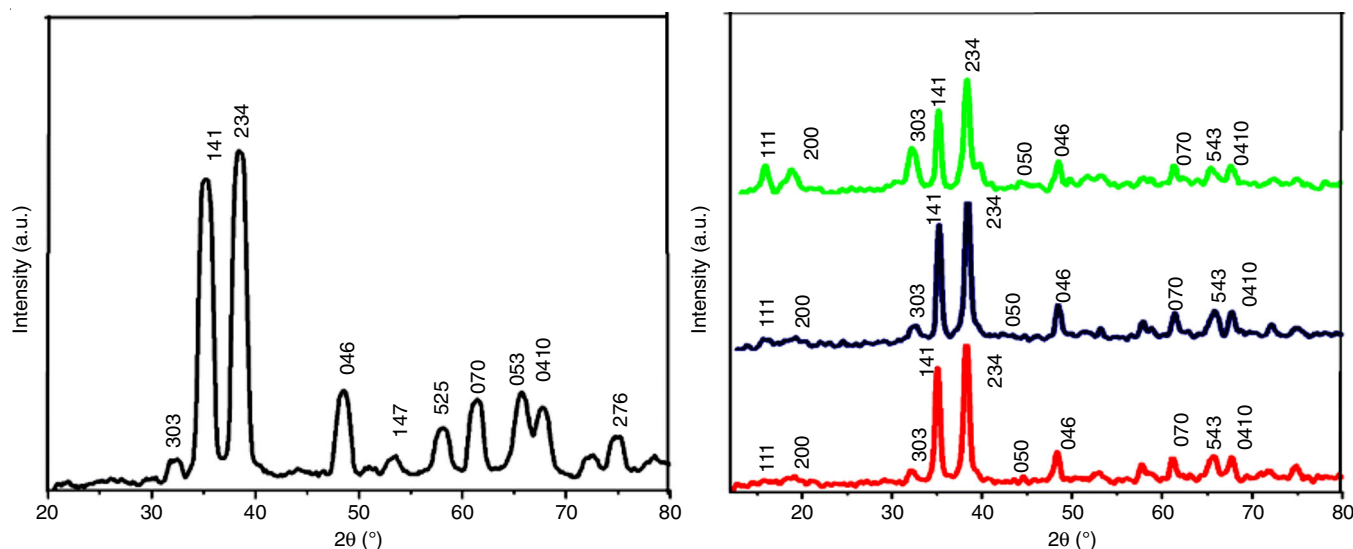

Fig. 1. XRD pattern of (a) CuO, (b) 30% Ni-composite, (c) 40% Ni-composite, and (d) 50% Ni-composite CuO nanoparticles

may disturb within neighboring ions [21]. Hence, it can be concluded that Ni^{2+} ions are formed on the host structure as composite ions, which changed the crystal structure from orthorhombic to cubic [22]. Further, the ionic radius of Ni^{2+} (0.69 Å) is lesser than that of Cu^{2+} (0.73 Å), which leads to the decrease in crystallite size for Ni composite concentration [23]. The various parameters for average crystallite size were calculated by Debye-Scherrer's equation [24]:

$$D = \frac{k \times \lambda}{\beta \cos \theta} \qquad (1)$$

where k = the shape factor of approximate value 0.9, λ = wavelength of Cu$K\alpha$ radiation (λ = 1.5406 Å), β = FWHM and θ = diffraction angle (º).

The dislocation density (δ) of the electrode material was given by the formula [24]:

$$\delta = \frac{1}{D^2} \qquad (2)$$

Microstrain (ε) was the calculated by eqn. 3 [25]:

$$\varepsilon = \frac{\beta \cos \theta}{4} \qquad (3)$$

Table-1 displays the calculated parameters from the XRD data of crystal size, dislocation density and microstrain. In Ni@CuO composites, the crystallite size reduced to16.60 nm, 14.64 nm and 11.37 nm when the Ni ratio increased to 30%, 40% and 50%, respectively. Significantly, the crystallite size decreased with increased microstrain. The minimum crystallite size obtained this work (11.37 nm) considers for further investigations. The small crystalline size leads to high specific capacitance and good cycle stability of the prepared electrode materials [26].

TABLE-1			
Sample	Crystallite size (nm)	Dislocation density, δ (lines/m^2)	Microstrain (ε) $\times 10^{-3}$
CuO	13.23	5.715	2.622
30% Ni	16.60	2.454	0.835
40% Ni	14.64	2.614	1.868
50% Ni	11.37	2.966	3.144

FT-IR studies: To study the presence of chemical bonding, the FTIR spectra of bare CuO and Ni@CuO are recorded and shown in Fig. 2a-d. Generally, the absorption bands are below 1000 cm^{-1}, which corresponds to the metal oxide that arrived at the interatomic vibrations. The absorption peaks at 493 cm^{-1} and 610 cm^{-1} are ascribed to metal band (Cu-O stretching vibrations). The absorption peak at 750 cm^{-1} should be related to the Ni-O vibration that arises from 40% of the composite product [27]. The presence of the broad peaks around at 3427 cm^{-1} is owing to stretching vibration of water molecule. The absorption band located at 1650 cm^{-1} is usually ascribed to the bending modes of water molecules from atmosphere. The weak absorption band position at 2900 cm^{-1}, in all the samples are attributed to C-H bond as a stretching vibration [28-31].

Surface morphological studies: The different surface morphologies and particle sizes of the prepared Ni@CuO nano-
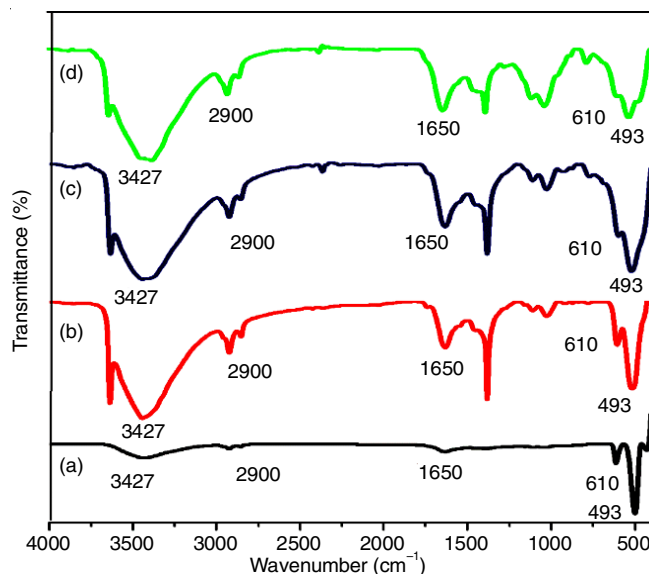

Fig. 2.   FTIR spectra of (a) CuO, (b) 30% Ni-composite, (c) 40% Ni-composite and (d) 50% Ni-composite CuO nanoparticles

composites were investigated using SEM technique. Fig. 3a-h shows the rod-like shape of CuO NPs and Ni@CuO nanocomposites provides a spherical like morphology. Further, the Ni incorporated host-material changed the structure and enhanced the surface area. Meanwhile, increasing Ni concentrations (30%, 40% and 50%) did not change the morphology [32,33]. The Ni composite products exhibited spherical shapes that were found to be non-uniform in size. It is also observed that heat treatment (hydrothermal method) has significant effect on the morphology of the synthesized products. The spherical nanoparticles were found to be grown in different orientations, however, the shape of spherical nanoparticle depends on the procedure and different relation parameters of the synthesis route. The Ni@CuO nanocomposites are obtained with an extensive yield and without existence of morphologically different structures. Accordingly, the observed Ni@CuO has a much larger smooth surface area than is needed for supercapacitors [34]. Fig. 4a-d illustrates the particle size of the bare and Ni@CuO (histogram images). The average particle sizes were found to be 15 nm (PEG-CuO), 14 nm (30% Ni), 11 nm (40% Ni) and 9.8 nm (50% Ni). These results are due to the electrostatic and van der Waals' interaction among the particles. EDX spectra of CuO and Ni@CuO nanocomposites are shown in Fig. 3i-j and confirmed the presence of Cu, Ni and O.

XPS studies: Fig. 5a-d indicates the spectra of copper, nickel and oxygen elements [35]. In XPS spectrum, Ni2p peaks found with doublet-fitted peaks at 855.85 and 856.52 eV are assigned to Ni 2p$_{2/3}$ and Ni 2p$_{1/2}$. XPS spectra exhibited the binding energies at 285.87 eV, 531.39 eV and 934.57 eV for C1s, O1s and Cu2p, respectively. The two components of O 1s spectrum shown at 530.86eV and 531.39 eV are related to oxygen bonds [36,37]. The XPS results are in line with the EDAX results.

Surface area analysis: The active surface area and pore size of PEG-CuO and Ni@CuO nanoparticles were distributed by nitrogen adsorption and desorption isotherm curves [38].
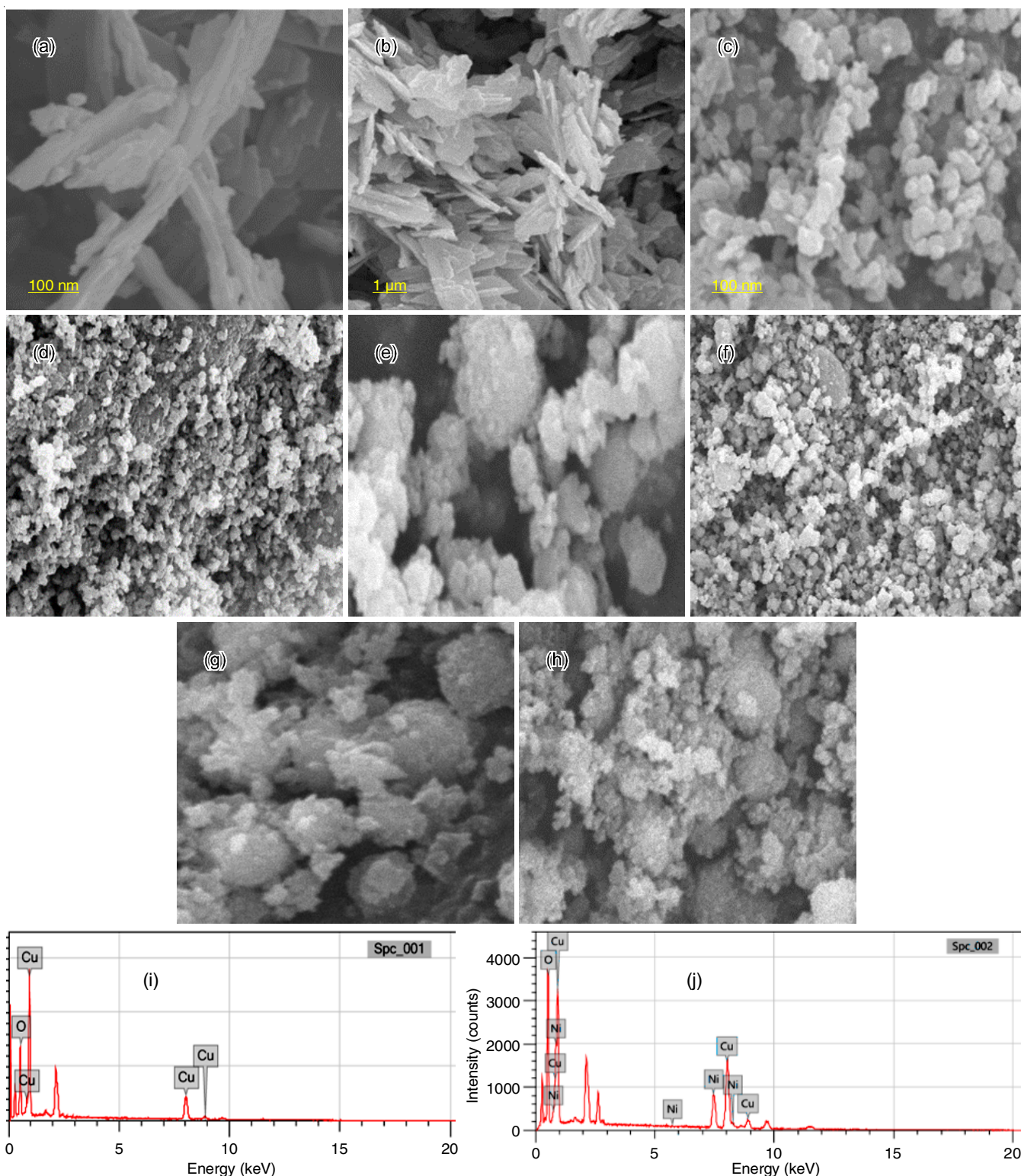
Fig. 3. SEM images of (a-b) CuO, (c-d) 30% Ni-composite, (e-f) 40% Ni-composite, and (g-h) 50% Ni-composite CuO nanoparticles. EDX images of (i) CuO and (n) Ni-composite CuO nanoparticles

Fig. 6a-d illustrate, the mesopore structure of the prepared nanomaterial is classified as type-IV as framed by IUPAC. The pore size and surface area of bare and Ni@CuO are found to be ~ 50 nm, 11.38 m^2 g^{-1} and ~ 58 nm, 17.58 m^2 g^{-1}. It is clearly observed that the surface area and pore size are significantly increased by the incorporation of Ni into CuO [39]. In high relative pressure, the N$_2$ adsorption and desorption curve indicates the existence of large mesoporous structure. A high active surface area observed for Ni@CuO is due to the lower crystal size. Furthermore, the surface area of Ni@CuO was increased owing to the enhancement of the pores, which yielded the high capacitance property [40].
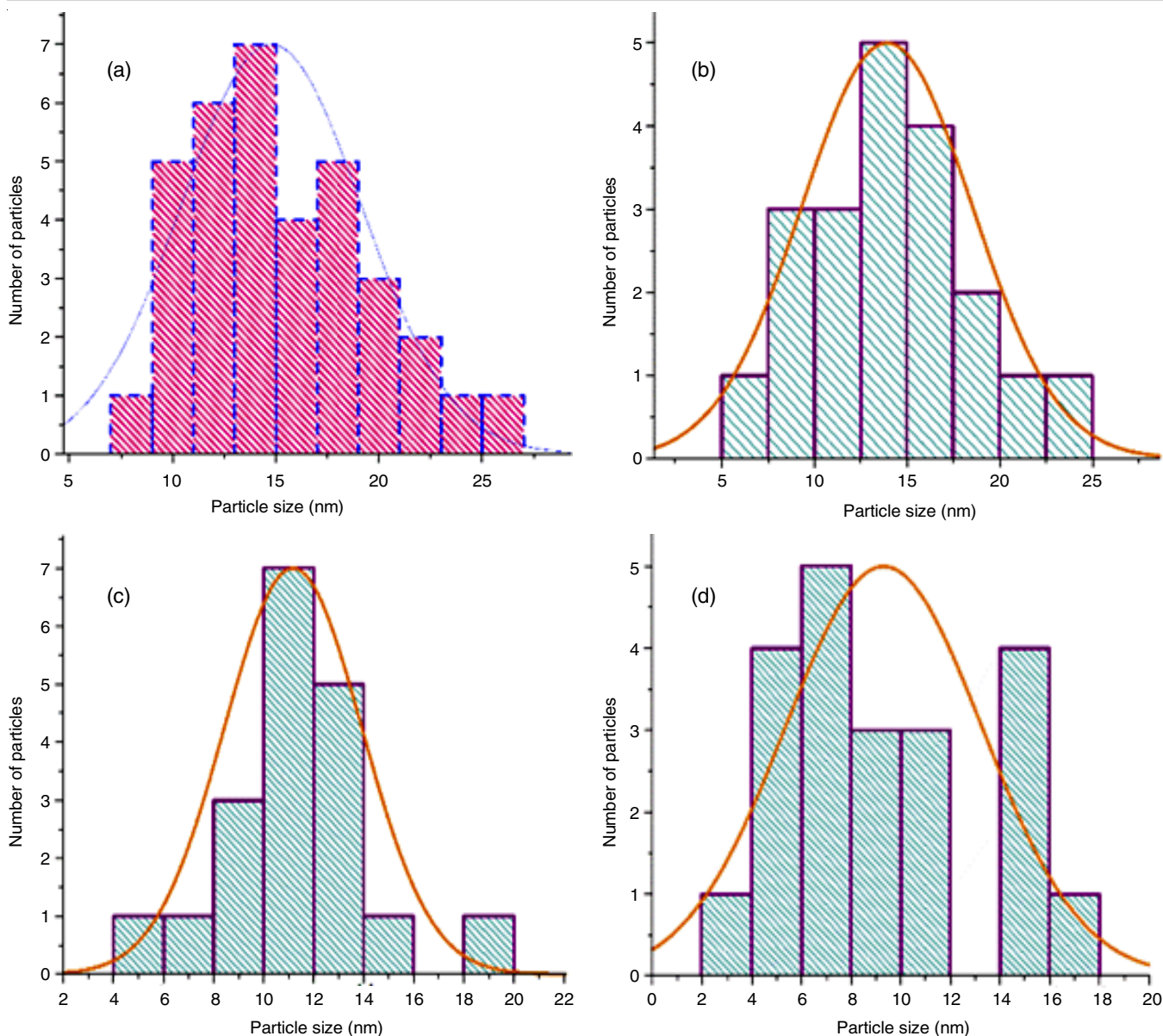
Fig. 4. Particle size distribution histograms (a) CuO (b-f) Ni-composite CuO nanoparticles

Electrochemical behaviour of Ni@CuO nanocomposites

Cyclic voltammetry: In this work, the cyclic voltammetry (CV) measurements for CuO NPs was performed using a three electrode cell combinations system 1 M Na_2SO_4 electrolyte [41]. Fig. 7a illustrates the CV curves of the prepared product at various scan rates from 10-100 mV s^{-1} in potential windows of 0.05-0.50 V. The principal characteristics of ideal materials are the rectangular shape, which exhibits the pseudocapacitive behaviour of the synthesized product.

The capacitance values of the prepared electrode material were calculated from the CV curves following the relation [42].

$$C_s = \frac{s}{mk\Delta V} \tag{4}$$

where s = the specific area of CV curve, m = mass of active electrode, k = the scan rate (mV/s) and ΔV = the potential window.

The C_{sp} of bare and composite are found to be 297, 275, 251, 186 and 153 F g^{-1} and 374 F g^{-1}, 347 F g^{-1}, 320 F g^{-1}, 298 Fg^{-1}, 273 F g^{-1} at diverse scan rates of 10-100 mV s^{-1}. However, the obtained specific capacitance values continuously reduced in the CV loop with increasing scan rates. In this case, the electrode reacts with the working electrode in a short time owing to the powerlessness of ions that could not access the inner active site since they were unable to get sufficient time [43]. These results proved that the Ni@CuO nanocomposites are more suitable for supercapacitor applications than PEG-CuO nanoparticles [43].

Galvanostatic charge-discharge studies: The GCD curves were recorded in a 1 M Na_2SO_4 with various current density (1, 2, 3 and 4 A g^{-1}). The charging/discharging curves were almost symmetrical triangular shapes and also exhibit a good linear variation (Fig. 7c-d), which proved excellent electrochemical performance [33].
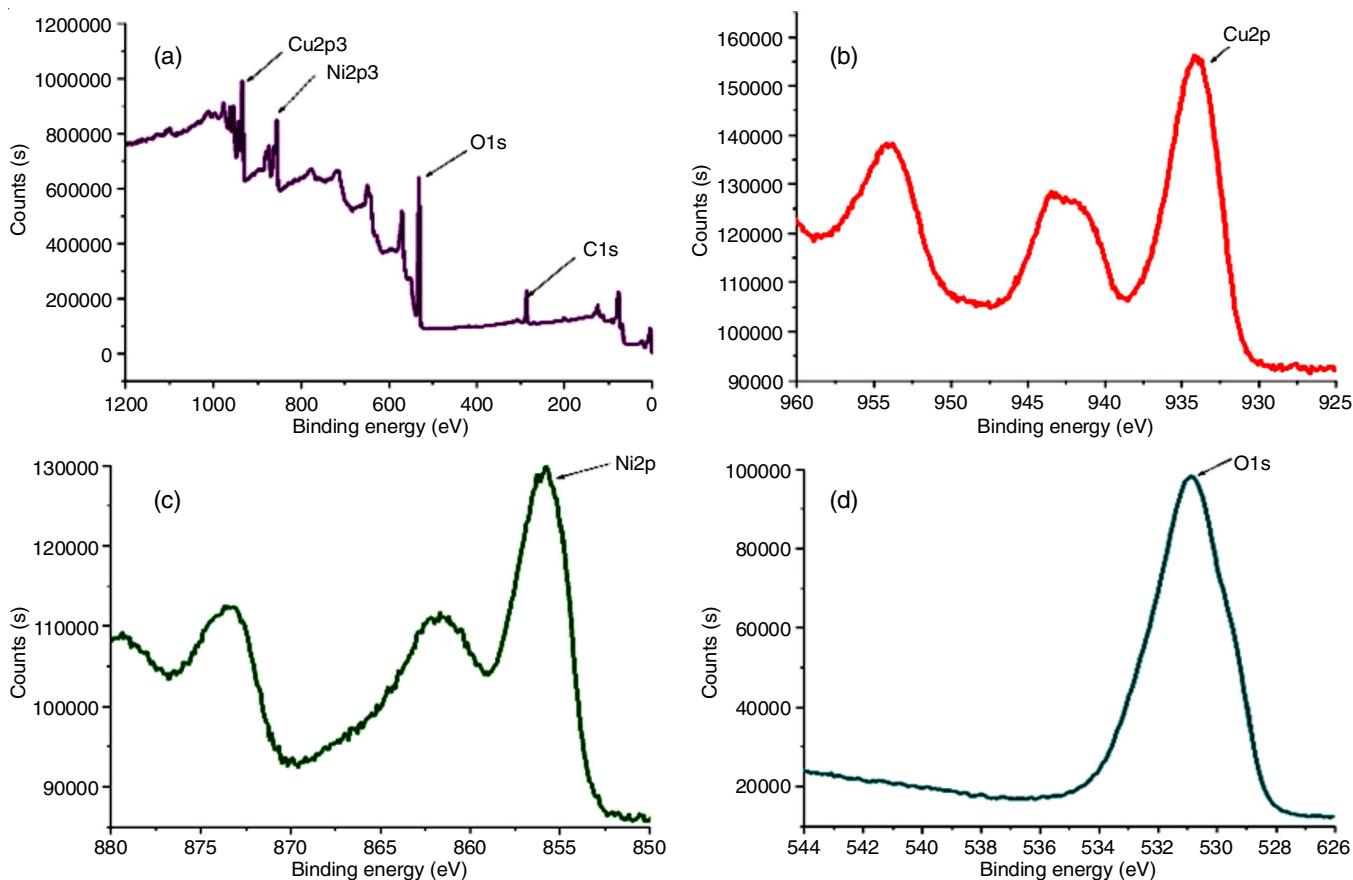
Fig. 5. (a) XPS survey spectra of Ni composite CuO nanoparticles and (b) core level spectra of Cu 2p, (c) Ni 2p and (d) O 1s
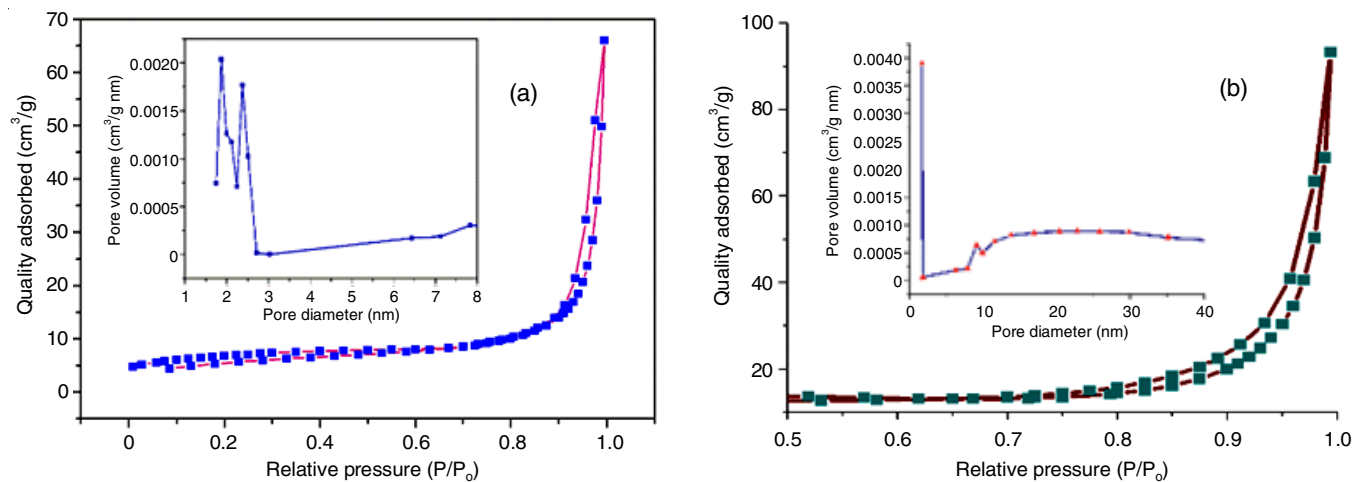

Fig. 6. (a and b) Nitrogen adsorption and desorption isotherms and the corresponding pore size distribution curve (inset) of CuO and Ni-composite CuO nanoparticles

From the GCD curves, the C_{sp} values of prepared nano-materials can be calculated using eqn. 5 [44]:

$$C_{sp} = \frac{I \times \Delta t}{m \times \Delta v}$$ (5)

The applied current (mA), the discharge time of GCD curves (s), the applied potential windows (V) and the mass of active material (mg) are I, Δt, ΔV and m, respectively.

The GCD curves (Fig. 7c-d) clearly indicate the pseudo-capacitance behaviour of Ni@CuO composite material. The C_{sp} values of 153, 147, 110 and 87 F g^{-1} (PEG-CuO) and 366,

339, 317 and 289 F g^{-1} (Ni@CuO) at diverse current densities of 1, 2, 3 and 4 A g^{-1}. The obtained capacitance value decreased with increased current density [45,46]. Fig. 7 (Ni@CuO) exposes a superior rate capability of 88.54%. The outstanding cyclic stability of the Ni@CuO than PEG-CuO nanomaterial can be mainly determined by its spherical-like structure and low crys-tallite size, which provide a suitable active surface area for ion transition. These results showed that the Ni@CuO nanocom-posites active electrode (mesoporous structure) is a promising candidate for electrochemical applications [47].
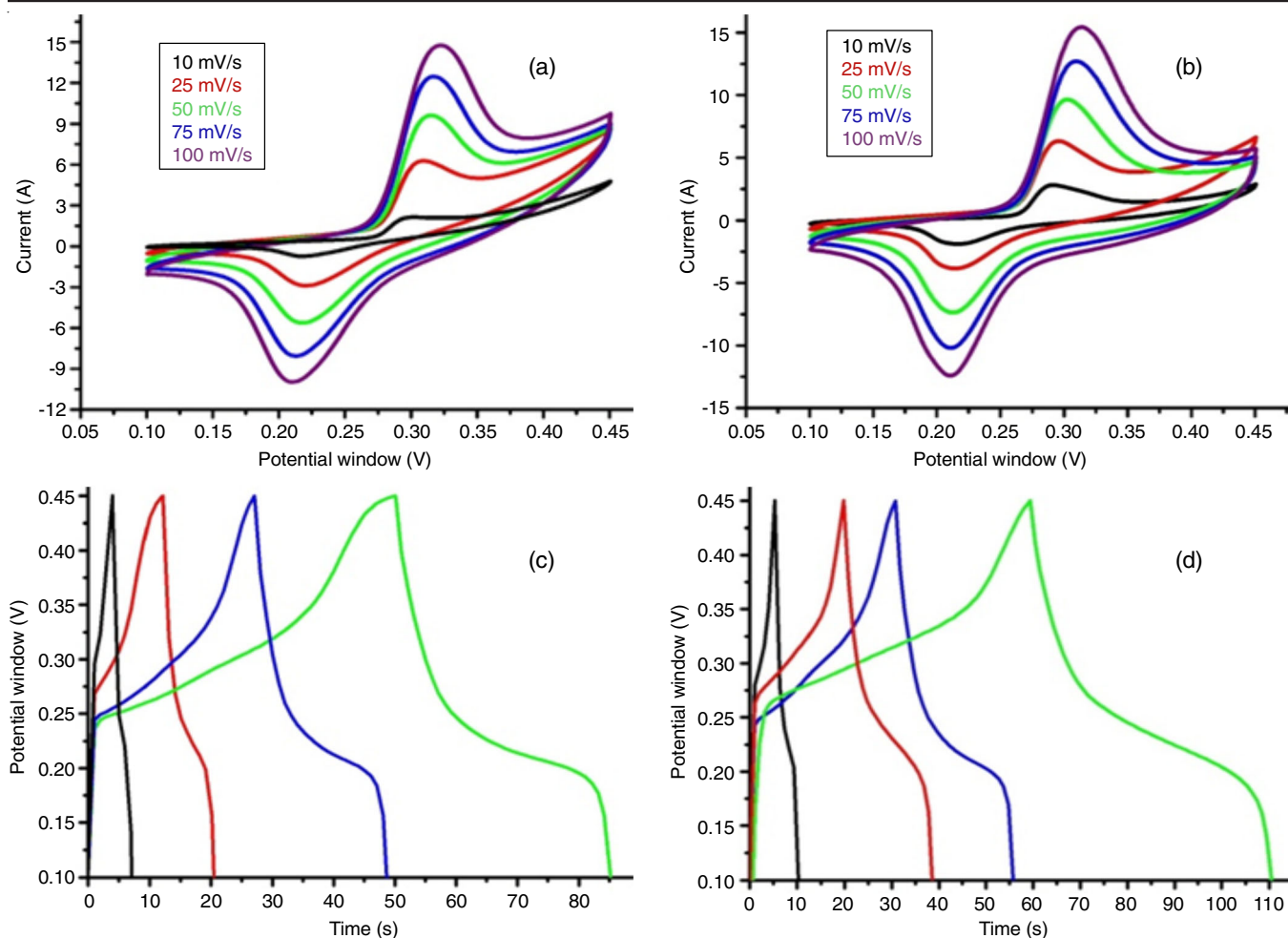
Fig. 7. CV curve of (a) CuO and (b) Ni (50%)-composite PEG assisted CuO, GCD curves of (c) CuO and (d) Ni (50%)-composite CuO
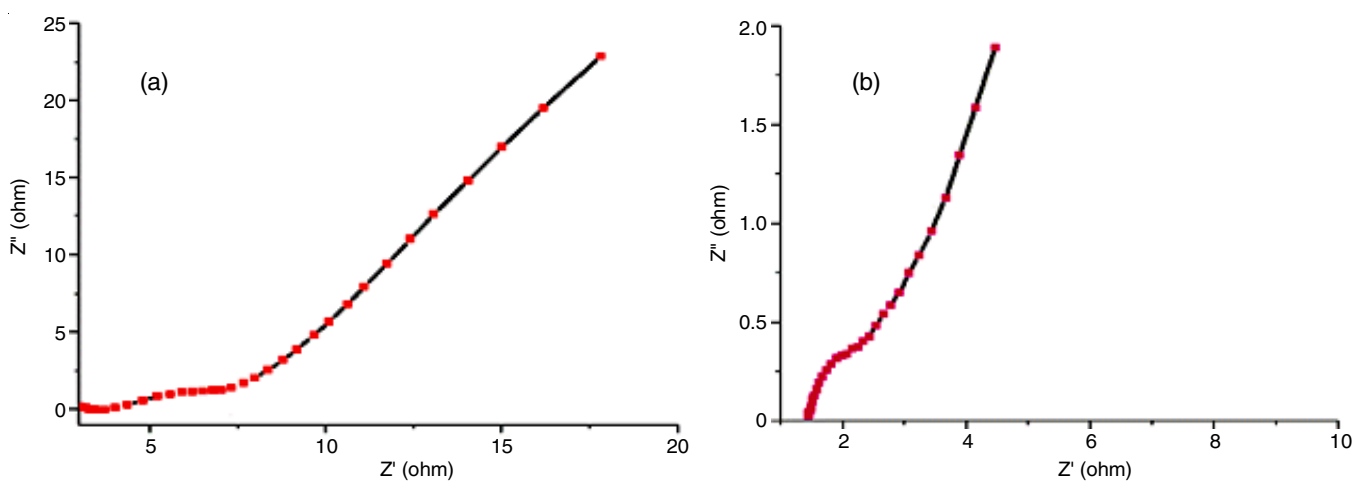

Fig. 8. (a) Nquist plot of CuO nano rod electrode and (b) Nquist plot of spherical like

EIS studies: The electrical conductivity and ion transfer properties of the prepared electrodes were investigated by the EIS technique. In the high-frequency region, the semi-circle was depressed, which corresponds to electrolyte resistance caused by Faradic reaction (Fig. 8a-b). A vertical linear spike is predicted along the imaginary axis in low frequency areas that results indicate pseudocapacitance characteristic features of the product [48,49]. As shown in figure, the semi-circle diameter for Ni@CuO is much smaller than that of CuO. The prepared Ni@CuO nanomaterial has outstanding performance for electrochemical applications.

Cycle stability: To assess the cycle stability of the prepared Ni@CuO electrode material and investigate its potential applications, GCD profiles were conducted over 1,000 cycles

at a current density of 0.25 A g^{-1}. According to Fig. 9, the Ni@CuO electrode exhibits exceptional cycling performance, with almost 88.54% capacitance retention up to 1,000 cycles. The result indicated that the reduced particle size, accessible surface area and shorter ion/electron transfer channels of Ni@CuO spherical structure could be suitable candidates for the electrochemical applications [50,51]. The capacitance retention of Ni@CuO (88.54%) composite is higher than PEG-CuO (77.24%). Additionally, the synthesized nanoparticles demonstrated improved mechanical power and long term charge-discharge with exceptional cycling capability.
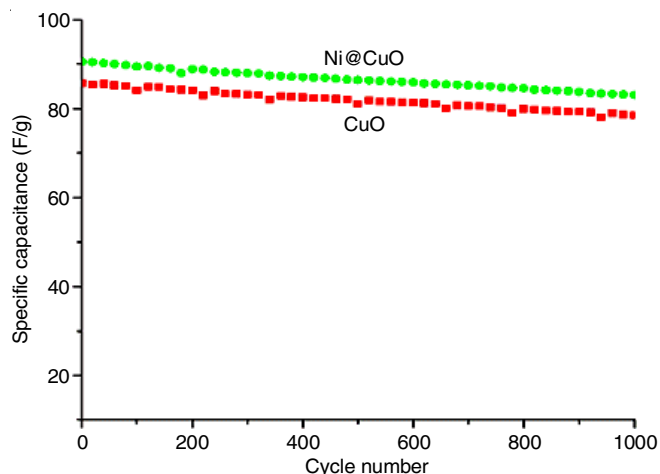

Fig. 9. Cycle stability and capacitance retention of CuO and Ni composite CuO electrode

Conclusion

In conclusion, a simple hydrothermal route was used to synthesize PEG-CuO and Ni@CuO nanocomposites with controlled crystal size and morphology. The crystal structure, morphology, chemical bonding and electrochemical behaviour of both nanostructures were thoroughly investigated. The XRD patterns indicated the cubic phase structure and the calculated crystallite size of 11.37 nm for (50%) Ni@CuO. The spherical like surface morphology of the composite products were further confirmed by SEM. The BET results distributed the enhanced active surface area of prepared product. The Ni@CuO showed a C$_{sp}$ value of 374 F g^{-1} at 10 mV s^{-1} and the capacitance retention of 88.54% after 1,000 cycles at 0.25 A g^{-1}.

CONFLICT OF INTEREST

The authors declare that there is no conflict of interests regarding the publication of this article.

REFERENCES

1. X. Su, G. Feng, L. Yu, Q. Li, H. Zhang, W. Song and G. Hu, *J. Mater. Sci. Mater. Electron.*, **30**, 3545 (2019);
https://doi.org/10.1007/s10854-018-00632-y
2. S.X. Wang, C.C. Jin and W.J. Qian, *J. Alloys Compd.*, **615**, 12 (2014);
https://doi.org/10.1016/j.jallcom.2014.06.149
3. L. Attou, B. Jaber and H. Ez-Zahraouy, *Appl. Phys.*, *A Mater. Sci. Process.*, **125**, 560 (2019);
https://doi.org/10.1007/s00339-019-2858-4
4. Z. Zhu and Z. Xu, *Renew. Sustain. Energy Rev.*, **134**, 110308 (2020);
https://doi.org/10.1016/j.rser.2020.110308
5. P. Sharma and V. Kumar, *Physica B*, **619**, 413212 (2021);
https://doi.org/10.1016/j.physb.2021.413212
6. S.G. Sayyed, A.V. Shaikh, U.P. Shinde, P. Hiremath and N. Naik, *J. Mater. Sci.: Mater. Electron.*, **34**, 1361 (2023);
https://doi.org/10.1007/s10854-023-10738-7
7. M. Czagany, S. Hompoth, A.K. Keshri, N. Pandit, I. Galambos, Z. Gacsi and P. Baumli, *Materials*, **17**, 702 (2024);
https://doi.org/10.3390/ma17030702
8. B. Saravanakumar, C. Radhakrishnan, M. Ramasamy, R. Kaliaperumal, A.J. Britten and M. Mkandawire, *Results Phys.*, **13**, 102185 (2019);
https://doi.org/10.1016/j.rinp.2019.102185
9. S. Chatterjee, A. Ray, M. Mandal, S. Das and S.K. Bhattacharya, *J. Mater. Eng. Perform.*, **29**, 8036 (2020);
https://doi.org/10.1007/s11665-020-05261-3
10. I. Shaheen, I. Hussain, T. Zahra, M.S. Javed, S.S.A. Shah, K. Khan, M.B. Hanif, M.A. Assiri, Z. Said, W. Ul Arifeen, B. Akkinepally and K. Zhang, *J. Energy Storage*, **72E**, 108719 (2023);
https://doi.org/10.1016/j.est.2023.108719
11. C. Chen, K. Xu, X. Ji, B. Zhang, L. Miao and J. Jiang, *J. Mater. Chem. A Mater. Energy Sustain.*, **3**, 12461 (2015);
https://doi.org/10.1039/C5TA01930C
12. J. Huang, B.G. Sumpter and V. Meunier, *Angew. Chem., Int. Ed.*, **47**, 520 (2008);
https://doi.org/10.1002/anie.200703864
13. J. Zhang, Y. Cui, Q. Qin, G. Zhang, W. Luo and W. Zheng, *Chem. Eng. J.*, **331**, 326 (2018);
https://doi.org/10.1016/j.cej.2017.08.089
14. J. Toupin, H. Strubb, S. Kressman, V. Artero, N. Krins and C. Laberty-Robert, *J. Sol-Gel Sci. Technol.*, **89**, 255 (2019);
https://doi.org/10.1007/s10971-018-4896-3
15. L. Kunhikrishnan and R. Shanmugam, *J. Mater. Sci. Mater. Electron.*, **31**, 21528 (2020);
https://doi.org/10.1007/s10854-020-04665-0
16. J. Lu, W. Xu, S. Li, W. Liu, M.S. Javed, G. Liu and C. Hu, *J. Mater. Sci.*, **53**, 739 (2018);
https://doi.org/10.1007/s10853-017-1493-8
17. E. Keles, M. Yildirim, T. Öztürk and O.A. Yildirim, *Mater. Sci. Semicond. Process.*, **110**, 104959 (2020);
https://doi.org/10.1016/j.mssp.2020.104959
18. M.S. Alqahtani, N.M.A. Hadia and S.H. Mohamed, *Optik*, **173**, 101 (2018);
https://doi.org/10.1016/j.ijleo.2018.08.016
19. J. Qian, X. Guo, T. Wang, P. Liu, H. Zhang and D. Gao, *Appl. Catal. B*, **250**, 71 (2019);
https://doi.org/10.1016/j.apcatb.2019.03.021
20. S.K. Nath, S. Maitra, S. Mukherjee and S. Kumar, *Constr. Build. Mater.*, **111**, 758 (2016);
https://doi.org/10.1016/j.conbuildmat.2016.02.106
21. J. Singh, R. Kumar, V. Verma and R. Kumar, *Ceram. Int.*, **46**, 24071 (2020);
https://doi.org/10.1016/j.ceramint.2020.06.185
22. A.A. Manoharan, R. Chandramohan, R. David Prabu, S. Valanarasu, V. Ganesh, M. Shkir, A. Kathalingam and S. AlFaify, *J. Mol. Struct.*, **1171**, 388 (2018);
https://doi.org/10.1016/j.molstruc.2018.06.018
23. V. Kumari, S. Yadav, J. Jindal, S. Sharma, K. Kumari and N. Kumar, *Adv. Powder Technol.*, **31**, 2658 (2020);
https://doi.org/10.1016/j.apt.2020.04.033
24. Z.R. Parekh, S.H. Chaki, A.B. Hirpara, G.H. Patel, R.M. Kannaujiya, A.J. Khimani and M.P. Deshpande, *Physica B*, **610**, 412950 (2021);
https://doi.org/10.1016/j.physb.2021.412950
25. A.R. Bushroa, R.G. Rahbari, H.H. Masjuki and M.R. Muhamad, *Vacuum*, **86**, 1107 (2012);
https://doi.org/10.1016/j.vacuum.2011.10.011
26. A.T. Babu and R. Antony, *J. Environ. Chem. Eng.*, **7**, 102840 (2019);
https://doi.org/10.1016/j.jece.2018.102840
27. T. Munawar, F. Iqbal, S. Yasmeen, K. Mahmood and A. Hussain, *Ceram. Int.*, **46**, 2421 (2020);
https://doi.org/10.1016/j.ceramint.2019.09.236

28. M.Z. Ishaque, Y. Zaman, A. Arif, A.B. Siddique, M. Shahzad, D. Ali, M. Aslam, H. Zaman and M. Faizan, *RSC Adv.*, **13**, 30838 (2023); https://doi.org/10.1039/D3RA05170F

29. S. Sivakumar and L.N. Prabu, *Mater. Today Proc.*, **47**, 52 (2021); https://doi.org/10.1016/j.matpr.2021.03.528

30. N. Senthilkumar, V. Venkatachalam, M. Kandiban, P. Vigneshwaran, R. Jayavel and I. Vetha Potheher, *Physica E*, **106**, 121 (2019); https://doi.org/10.1016/j.physe.2018.10.027

31. S.B. Ubale, S.B. Kale, V.J. Mane, U.M. Patil and C.D. Lokhande, *J. Electroanal. Chem.*, **897**, 115589 (2021); https://doi.org/10.1016/j.jelechem.2021.115589

32. M.A. Dar, D. Govindarajan and G.N. Dar, *J. Mater. Sci. Mater. Electron.*, **32**, 20394 (2021); https://doi.org/10.1007/s10854-021-06550-w

33. K. Ashokkumar, S. Dhanapandian, S. Suthakaran and N. Krishnakumar, *Mater. Technol.*, **37**, 2861 (2024); https://doi.org/10.1080/10667857.2022.2083483

34. A. Zhang, W. Zheng, Z. Yuan, J. Tian, L. Yue, R. Zheng, D. Wei and J. Liu, *Chem. Eng. J.*, **380**, 122486 (2020); https://doi.org/10.1016/j.cej.2019.122486

35. J.W. Ha, J. Oh, H. Choi, H. Ryu, W.J. Lee and J.S. Bae, *J. Ind. Eng. Chem.*, **58**, 38 (2018); https://doi.org/10.1016/j.jiec.2017.09.004

36. Q. Do, H. An, G. Wang, G. Meng, Y. Wang, B. Liu, J. Wang and F. Wang, *Corros. Sci.*, **147**, 246 (2019); https://doi.org/10.1016/j.corsci.2018.11.017

37. N. Budhiraja, Sapna, V. Kumar, M. Tomar, V. Gupta and S.K. Singh, *J. Inorg. Organomet. Polym. Mater.*, **29**, 1067 (2019); https://doi.org/10.1007/s10904-018-0995-4

38. J. Guilera, J. Del Valle, A. Alarcón, J.A. Díaz and T. Andreu, *J. CO2 Util.*, **30**, 11 (2019); https://doi.org/10.1016/j.jcou.2019.01.003

39. S. Asaithambi, P. Sakthivel, M. Karuppaiah, R. Yuvakkumar, T. Ahamad, K. Balamurugan, M.A.M. Khan, G. Ramalingam, M.K.A. Mohammed and G. Ravi, *J. Energy Storage*, **36**, 102402 (2021); https://doi.org/10.1016/j.est.2021.102402

40. V. Kakani, S. Ramesh, H.M. Yadav, A. Kumar, S. Shinde, S. Sandhu, L.N. Dang Quang, H.S. Kim, H.-S. Kim, H. Kim and C. Bathula, *J. Alloys Compd.*, **847**, 156411 (2020); https://doi.org/10.1016/j.jallcom.2020.156411

41. S.K. Shinde, S.M. Mohite, A.A. Kadam, H.M. Yadav, G.S. Ghodake, K.Y. Rajpure, D.S. Lee and D.-Y. Kim, *J. Electroanal. Chem.*, **850**, 113433 (2019); https://doi.org/10.1016/j.jelechem.2019.113433

42. S. Arunachalam, B. Kirubasankar, V. Murugadoss, D. Vellasamy and S. Angaiah, *New J. Chem.*, **42**, 2923 (2018); https://doi.org/10.1039/C7NJ04335J

43. L. Yan, L. Niu, C. Shen, Z. Zhang, J. Lin, F. Shen, Y. Gong, C. Li, X. Liu and S. Xu, *Electrochim. Acta*, **306**, 529 (2019); https://doi.org/10.1016/j.electacta.2019.03.174

44. A. Ray, A. Roy, M. Ghosh, J. Alberto Ramos-Ramón, S. Saha, U. Pal, S.K. Bhattacharya and S. Das, *Appl. Surf. Sci.*, **463**, 513 (2019); https://doi.org/10.1016/j.apsusc.2018.08.259

45. H. Chen, J. Wang, F. Liao, X. Han, C. Xu and Y. Zhang, *Ceram. Int.*, **45**, 8008 (2019); https://doi.org/10.1016/j.ceramint.2019.02.010

46. B. Rani and N.K. Sahu, *Diamond Rel. Mater.*, **108**, 107978 (2020); https://doi.org/10.1016/j.diamond.2020.107978

47. S. Huo, X. Zhang, B. Liang, Y. Zhao and K. Li, *J. Power Sources*, **450**, 227612 (2020); https://doi.org/10.1016/j.jpowsour.2019.227612

48. D. Govindarajan, F.J. Johanson, V. Uma Shankar, M.J. Salethraj and R. Gopalakrishnan, *J. Mater. Sci. Mater. Electron.*, **32**, 19434 (2021); https://doi.org/10.1007/s10854-021-06460-x

49. K.M. Racik, A. Manikandan, M. Mahendiran, P. Prabakaran, J. Madhavan and M.V.A. Raj, *Physica E*, **119**, 114033 (2020); https://doi.org/10.1016/j.physe.2020.114033

50. S.Y. Attia, Y.F. Barakat, H.H. Hassan and S.G. Mohamed, *J. Energy Storage*, **29**, 101349 (2020); https://doi.org/10.1016/j.est.2020.101349

51. A.E. Elkholy, F. El-Taib Heakal and N.K. Allam, *Electrochim. Acta*, **296**, 59 (2019); https://doi.org/10.1016/j.electacta.2018.11.038